ARCTIC
VOL. 53, NO. 4 (DECEMBER 2000) P. 341–358

Variability of Arctic Sea Ice: The View from Space, An 18-Year Record

CLAIRE L. PARKINSON[1]

(*Received 8 December 1998; accepted in revised form 5 September 1999*)

ABSTRACT. A recently compiled 18-year record (1979 to 1996) of sea ice concentrations derived from four passive-microwave satellite instruments has allowed the quantification of a variety of measures of Arctic sea ice variability. Earlier maps generated using data through August 1987 have been updated to 18-year summaries of the annual range of sea ice distributions, the interannual variability of average monthly sea ice distributions, the frequency of sea ice coverage over the 18 years, the length of the sea ice season, and trends in the length of the sea ice season. Linear least squares trends over the 18-year record show the sea ice season to have lengthened over some sizeable regions, especially in the Bering Sea, Baffin Bay, Davis Strait, the Labrador Sea, and the Gulf of St. Lawrence, but to have shortened over a much larger area, including the Sea of Okhotsk, the Greenland Sea, the Barents Sea, and all the seas along the north coast of Russia. The area with trends showing sea ice seasons shortening by over 0.5 days/year is 7.5×10^6 km^2, over 2.5 times the area experiencing a lengthening of the sea ice season by over 0.5 days/year. Neither the shortening nor the lengthening, however, is uniform or monotonic over the 18-year record. Instead, the ice cover exhibits widespread interannual variability, not just in the length of the sea ice season but for each month—a fact well illustrated by the monthly average September ice coverage, which was at its lowest extent in 1995 but at its second highest one year later, in the final year of the record. The maps of ice frequency and ice variability can help identify how anomalous individual years are. In some cases, they can help forestall unnecessary concern over seemingly unusual conditions which, upon examination of the maps, are found to fall well within the observed variability.

Key words: Arctic sea ice, climate change, polar climate, remote sensing

RÉSUMÉ. Grâce à un dossier compilant 18 années d'étude (de 1979 à 1996) sur les concentrations de glace marine mesurées par quatre instruments à hyperfréquences passives portés sur des satellites, on a pu quantifier diverses mesures de la variabilité de la glace marine dans l'Arctique. Les premières cartes créées à l'aide de données allant jusqu'en août 1987 ont été mises à jour sous forme de résumés (portant sur une période de18 ans) de la superficie annuelle des distributions de glace marine, de la variabilité interannuelle de la moyenne mensuelle des distributions de glace marine, de la fréquence de la couverture de glace marine au cours des 18 années, de la durée de la saison de glace marine et des tendances dans cette même durée. Une analyse des tendances, par la méthode linéaire des moindres carrés, enregistrées sur 18 ans montre que la saison de glace marine est devenue plus longue dans certaines régions assez vastes, surtout dans la mer de Béring, la baie de Baffin, le détroit de Davis, la mer du Labrador et le golfe du Saint-Laurent, mais qu'elle a raccourci dans une zone bien plus étendue, qui comprend la mer d'Okhotsk, la mer de Norvège, la mer de Barents et toutes les eaux longeant la côte nord de Russie. La région où se manifestent les tendances au raccourcissement de la saison de glace marine de 0,5 jour/an s'étend sur 7,5 x 10^6 km^2, soit plus de 2,5 fois l'étendue où se manifeste une extension de la saison de glace marine de 0,5 jour/an. Mais ni le raccourcissement ni l'extension ne sont uniformes ou monotones au cours des 18 années d'études. La couverture de glace affiche, au contraire, une variabilité interannuelle généralisée, non seulement dans la longueur de la saison de glace marine, mais pour chaque mois – fait qu'illustre bien la moyenne mensuelle de la couverture de glace pour le mois de septembre, moyenne qui était à son minimum en 1995, mais à son maximum de second rang un an plus tard, durant l'année finale de l'enregistrement. Les cartes de fréquence de la glace et de variabilité de la glace peuvent montrer les anomalies d'une année à l'autre. Dans certains cas, ces cartes peuvent aider à prévenir d'inutiles soucis quant aux conditions apparemment inhabituelles qui, si l'on étudie les cartes, se situent parfaitement dans la fourchette de variabilité observée.

Mots clés: glace marine arctique, changement climatique, climat polaire, télédétection

Traduit pour la revue *Arctic* par Nésida Loyer.

INTRODUCTION

Background

Sea ice is a major element in the environment of polar marine plant and animal life, including a vast assortment of life forms that live within the ice itself (e.g., Horner, 1989; Spindler, 1990; Melnikov, 1997). Algae colonize the ice, sometimes to the tune of millions in individual ice floes, with a biomass that can be as high as 100 mg of chlorophyll *a* per square meter (Gradinger, 1995). The algae are feasted upon by protozoans, crustaceans, and

[1] Oceans and Ice Branch/Code 971, NASA Goddard Space Flight Center, Greenbelt, Maryland 20771, U.S.A.; clairep@neptune.gsfc.nasa.gov

nematodes, most smaller than 1 mm (Gradinger, 1995). One cubic meter of the ice may contain over 100 000 such creatures, and densities are particularly high near the bottom surface (Melnikov, 1997). Although biomass tends to be low in the water underneath the permanent ice pack, high phytoplankton and zooplankton concentrations are frequently found in the water of the marginal ice zones and polynyas, or open water areas within the ice cover (Smith and Sakshaug, 1990; Smith and Schnack-Schiel, 1990). The resulting availability of food, along with the platform provided by the ice surface, makes these areas popular for numerous species of birds and marine mammals (Ainley and DeMaster, 1990; Stirling, 1997). Among the larger animals taking advantage of the ice platform are seals, who can give birth and nurse their pups there and, more routinely, rest and escape from whale predators. Polar bears live on the ice sometimes for months at a time, roaming for hundreds of kilometres, often in search of prey or mates (Stirling and Derocher, 1993). Since polar bears feed largely on seals, they tend to inhabit regions in the vicinity of seal populations (Stirling and Derocher, 1993). However, polar bears feed predominantly from the platform of sea ice floes, and so they require the presence of ice thick enough to bear their weight. Whales, in contrast, are hindered by the ice and rely upon leads and open water as they travel in polar oceans. Bowhead whales, for instance, use the shoreleads of the Beaufort Sea in their annual migration from the Bering Sea to their breeding grounds in the central and eastern Canadian Arctic (Massom, 1988). Any major changes in sea ice distributions would affect all of these Arctic life forms, along with numerous others (e.g., see Ainley and DeMaster, 1990; Smith and Schnack-Schiel, 1990; Grebmeier et al., 1995; Stirling, 1997).

Observational records suggest that, on average over the past century, the earth's climate has warmed (Hansen and Lebedeff, 1987; Karl et al., 1994; Halpert and Bell, 1997). Other changes that have occurred in the climate system in harmony with the warming include glacier retreats in many of the glaciated regions of Europe (Williams and Ferrigno, 1993), Africa (Young and Hastenrath, 1991), and elsewhere (e.g., Williams and Ferrigno, 1989; Thompson et al., 1993) and sea level rise (Gornitz et al., 1982; Warrick et al., 1996), caused both by thermal expansion of the water as it warms and by the addition of water to the oceans as land ice either melts and flows into the oceans or enters the oceans as ice.

Calculations suggest that predicted future atmospheric warming will have significant impacts on the Arctic sea ice cover, noticeably reducing the ice thickness and ice concentration, or percent areal coverage of ice (Parkinson and Kellogg, 1979). Furthermore, ice reductions generate feedbacks that enhance the warming (Kellogg, 1975). In fact, calculations using the general circulation model (GCM) of the Goddard Institute for Space Studies suggest that as much as 37% of the simulated global temperature rise in the event of a doubling of atmospheric CO_2 results from sea ice changes and their feedbacks to the rest of the climate system (Rind et al., 1995).

However, records of Arctic sea ice are insufficient for a comprehensive analysis of ice coverage over the past century, as no feasible means of obtaining repeat measurements of the large-scale ice cover existed before the advent of satellite technology in the second half of the 20th century. Fortunately, that situation should be changed by the end of the 21st century: through satellites, we have begun to keep what should eventually be consistent, large-scale, long-term records of the Arctic sea ice cover. This paper uses the most complete record of large-scale Arctic sea ice coverage over the past two decades, that derived from satellite passive-microwave observations, to highlight some of what the satellites are revealing about Arctic sea ice variability.

The Satellite Passive-microwave Record

Satellite passive-microwave observations have proven tremendously valuable for monitoring sea ice coverage, for four central reasons: (1) At many microwave wavelengths, the radiative emissions of sea ice are markedly greater than those of the surrounding water. This contrast allows us to distinguish between ice, water, and ice/water mixtures on the basis of the amount of radiation recorded by the satellite. (2) The microwave radiation received by the satellite comes almost entirely from the earth system, so that, unlike data from visible wavelengths, which come predominantly from the sun, the passive-microwave data can be collected day or night. (3) At many microwave wavelengths, the data received by the satellite are largely unaffected by atmospheric conditions between the earth's surface and the satellite—another major advantage over observations from sensors operating at visible wavelengths, for which intervening clouds typically obscure the surface. For microwave observations, precipitating clouds can substantially affect the data, but nonprecipitating clouds generally do not. (4) Satellite passive-microwave instruments can measure the global sea ice cover every few days, with a resolution on the order of 25–50 km, providing adequate spatial resolution and extremely good temporal resolution for most climate-related studies.

The satellite passive-microwave record of Arctic ice began in December 1972, following the launch of the Electrically Scanning Microwave Radiometer (ESMR) on board NASA's Nimbus 5 satellite. The ESMR provided good-quality data for the Arctic for most of the period from January 1973 through October 1976, and these data were used to derive sea ice concentrations throughout the north polar region (Parkinson et al., 1987). However, the ESMR record contains only one channel of information, and this prevents the determination of distinctions among ice types and limits the accuracy of the derived ice concentrations to an estimated ± 15%. In addition, the record contains some major data gaps, one lasting three months. Nonetheless, the ESMR observations proved the effectiveness of passive-microwave technology for obtaining sea ice information from space under all lighting conditions and most

weather conditions. Of the more advanced passive-microwave instruments that succeeded the ESMR, the most important have been NASA's Nimbus 7 Scanning Multichannel Microwave Radiometer (SMMR), launched on 24 October 1978, and the sequence of Defense Meteorological Satellite Program (DMSP) Special Sensor Microwave Imagers (SSMIs), the first of which was launched on 19 June 1987. Both the SMMR and the SSMIs are multichannel instruments that allow a more accurate derivation of Arctic sea ice concentrations than was possible with the ESMR. The SMMR and SSMI records are also far less plagued by long data gaps than is the ESMR record. Together, the SMMR and SSMIs provide a fairly complete passive-microwave record of Arctic sea ice since October 1978. This record is used here as the data source for determining the variability of Arctic sea ice.

DATA

The data sources for the results presented in the following section are the Nimbus 7 SMMR and three DMSP SSMIs. The SMMR provided data every other day for most of the period from 26 October 1978 through 20 August 1987. The SMMR had ten data channels, three of which were used to determine sea ice concentrations through a formulation involving (a) the spectral gradient ratio between the vertically polarized data at a frequency of 18 GHz and the vertically polarized data at 37 GHz, (b) the ratio (termed the "polarization") of the difference to the sum of the vertically and horizontally polarized data at 18 GHz, and (c) a weather filter that simply sets all ice concentrations to 0 when the gradient ratio exceeds a preset cutoff of 0.07. Details of the algorithm can be found in Gloersen et al. (1992), as can monthly average maps of derived sea ice concentrations from November 1978 through August 1987.

The first SSMI, launched on the DMSP F8 satellite, provided daily data for most of the period from 9 July 1987 through 18 December 1991. The two subsequent SSMIs returning data used in this paper were those on board the DMSP F11 satellite and the DMSP F13 satellite. The F11 SSMI operated daily for most of the period from 3 December 1991 through 30 September 1995, and the F13 SSMI operated daily for most of the period from 3 May 1995 at least through 31 December 1996, the ending date for the compiled data set used here. The SSMI instruments have seven data channels, of which four are used in the sea ice calculations. Those four return horizontally polarized data at 19.35 GHz and vertically polarized data at 19.35 GHz, 22.235 GHz, and 37 GHz. For determination of sea ice concentrations, the 18 GHz channels on the SMMR instrument are much preferred over the 19.35 GHz channels that replaced them on the SSMIs, because the 19.35 GHz channels are more affected by atmospheric conditions. As a result, although the ice concentration calculation from the SSMI data follows the same basic formulation as the calculation from the SMMR data, the weather filter for the SSMI calculations is strengthened to incorporate the 22.235 GHz data as well as the gradient ratio between the 19.35 GHz and 37 GHz data. Details regarding these formulations can be found in Cavalieri et al. (1999).

Even though the passive-microwave data recorded by the satellite are not nearly as affected by atmospheric conditions as visible data are, wind, water vapor, and cloud liquid water all can affect the microwave radiative data and hence the calculated ice concentrations. Each of these elements tends to decrease the polarization used in the algorithm. Furthermore, winds tend to decrease the gradient ratio, and atmospheric water tends to increase it. The net effect of such interference is generally to increase the calculated ice concentration (Maslanik, 1992; Oelke, 1997). The weather filter used in the calculations effectively eliminates the resulting inaccurate calculation of ice presence in regions with no ice; however, it does not correct the weather-produced calculated increase in ice concentrations within the ice pack (Maslanik, 1992). Through radiative transfer modeling, Maslanik (1992) found that weather effects, in addition to causing increases in the total ice concentrations calculated using SMMR data, can cause even more substantial reductions in the calculated percentage of multiyear ice (ice that has survived a summer melt season). Oelke (1997) similarly calculates, for the SSMI data, that cloud liquid water and water vapor can cause increases in calculated ice concentrations of up to 10% and cause much larger decreases in multiyear ice fractions. This paper presents only the ice concentration totals, not the more questionable multiyear ice fractions.

Various technical differences in the four data sources (the SMMR and three SSMIs) have complicated the merging of the data records into a consistent combined data set. The primary difference is that the SMMR has 18 GHz channels in the 18–20 GHz range while the SSMIs have 19.35 GHz channels. Other differences include the orbital altitude of the satellite (ranging from 840 km for the DMSP F11 to 955 km for the Nimbus 7), the equatorial crossing times, the earth incidence angle (ranging from 50.2° for the SMMR to 53.3° for the F11 SSMI), and the effective field of view (which, for the 18 and 19.35 GHz channels, is 55 km × 65 km for the SMMR, 69 km × 43 km for the F8 SSMI, 67 km × 42 km for the F11 SSMI, and 70 km × 43 km for the F13 SSMI). These differences in the instruments and orbits mean that the data from the different instruments do not match precisely during the periods of data overlap. However, removing flaws in the data and tuning the ice concentration algorithms can greatly reduce the inconsistencies. With that in mind, a group at Goddard Space Flight Center undertook to create a consistent ice concentration record from the SMMR and SSMI data in the early 1990s. This effort, completed in 1998, involved removing clearly erroneous data, interpolating for missing data, correcting for instrument drifts, intercalibrating the sensors, and reducing false indications of sea ice arising

from atmospheric conditions and from land-to-ocean radiative spillover in the vicinity of coastal boundaries. Details regarding each of these corrections can be found in Cavalieri et al. (1999). The result is an 18.2-year SMMR/SSMI satellite-derived record of sea ice concentrations in both polar regions, covering the period from late October 1978 through the end of December 1996. The group effort included determination and analysis of regional and hemispheric sea ice extents (cumulative areas of all grid cells having calculated sea ice concentrations of at least 15%), and those results for the Arctic are presented in Parkinson et al. (1999). The current paper presents the 18-year variability in the spatial distributions of the Arctic ice cover using the same compiled SMMR/SSMI data set, which is available through the National Snow and Ice Data Center (NSIDC) in Boulder, Colorado.

All the data are mapped onto a common grid (grid cell size = 25 km × 25 km) overlaying a polar stereographic projection (NSIDC, 1992). Because of the specific near-polar orbits of the Nimbus 7 and DMSP satellites, the SMMR data do not extend poleward of 84.6°N and the SSMI data do not extend poleward of 87.6°N, although all other latitudes are covered.

Figures 1 and 2a provide illustrative samples of the passive-microwave data for a single date, 3 January 1996. Figure 1 provides images of the radiative data (converted to temperature units (K) termed "brightness temperatures") for two of the SSMI data channels, and Figure 2a provides an image of the derived sea ice concentrations. Figures 1a and 1b show a typical amount of missing data, color-coded as black. During the generation of the compiled ice concentration data set, the hundreds of isolated missing-data points (the black dots on Figures 1a and 1b) are eliminated through spatial interpolation on the brightness temperatures, whereas the larger blocks of missing data are eliminated through temporal interpolation on the ice concentrations. The one area of missing data that is not eliminated, and that hence appears on Figure 2a as well as on Figures 1a and 1b, is the circular area poleward of 87.6°N, from which no data were obtained because of the specific near-polar orbit of the DMSP satellite. Also visible on Figure 1a, in the upper left quadrant, are two scans of bad data, seen as streaks of out-of-place colors having the characteristic curved shape of the satellite scans. These scans of bad data, once identified, are treated as missing data and replaced by interpolated values.

Along most of its length, the location of the sea ice edge (visible in Figure 2a at the break between the lightest blue and the other coded colors) shows up clearly on both brightness temperature images of Figure 1. In Figure 1a, it occurs, along with the water/land boundaries, at the break between white and the other colors. In Figure 1b, it is less obvious but still clear to an experienced eye, occurring at the break between the greens/yellows and the browns/reds. This ready identification of the ice edge in the brightness temperature images, a result of the sharp contrast between the radiative emissions of ice and water at the two frequencies and polarizations being used, helps illustrate why the microwave data are so valuable for sea ice studies. It also suggests a robustness in the determination of overall ice coverage that far exceeds the robustness in the determination of ice concentrations, which are estimated (Gloersen et al., 1992) as being accurate to within about ± 7%.

Figure 2b provides a location map for the place names mentioned in the following sections.

RESULTS – ARCTIC SEA ICE VARIABILITY 1979–96

The SMMR/SSMI data record has been used to create a set of digital data and maps that show various aspects of sea ice variability over the 18-year period 1979–96. Except where otherwise noted, depiction of sea ice coverages is based on an ice concentration cutoff of 15%, meaning that the maps are color-coded to show ice extending to all pixels where the calculated ice concentration is ≥ 15% and to no pixels where the calculated ice concentration is less than 15%. (The ice concentration maps, e.g., Figs. 2a and 3, have a color scale in which the lowest ice concentration class is at 12–16%, so that the ice edge on these maps shows up at 12% ice concentration. In view of the small area covered by ice with monthly average concentrations in the 12–16% range [Figs. 2a and 3], these maps also closely identify where the calculated 15% ice edge lies.)

Intra-annual Range of Ice Coverage

Over the course of the 1979–96 SMMR/SSMI record, the average seasonal cycle of sea ice in the north polar region had ice extents ranging from a minimum of 7.0×10^6 km^2 in September to a maximum of 15.4×10^6 km^2 in March (Parkinson et al., 1999). In fact, minimum ice extent consistently occurred in September in each of the 18 years, and maximum ice extent occurred in March in all years except 1981, 1987, 1989, and 1996, when it occurred in February.

Figure 3 illustrates the intra-annual range of ice coverage by presenting monthly average ice concentration images for March and September of 1996, the final year of the 18-year record. Figure 4 incorporates data from each of the 18 years, presenting the average September ice coverages (with ≥ 15% ice concentration; labeled "Perennial Ice") and the average March ice coverages (with ≥ 15% ice concentration; identified on the figure as the combined regions of "Perennial Ice" plus "Seasonal Ice"). In the case of the 18-year averages (Fig. 4) and in each of the individual years (e.g., Fig. 3), the September ice is confined mostly to the Arctic Ocean and the Canadian Arctic Archipelago, whereas the March ice extends southward to cover (to an ice concentration of at least 15%) the entire Arctic Ocean, the Canadian Arctic Archipelago, Hudson Bay, and the Kara Sea, plus large portions of the Sea of Okhotsk, the Bering Sea, Baffin Bay, the far western Labrador Sea,

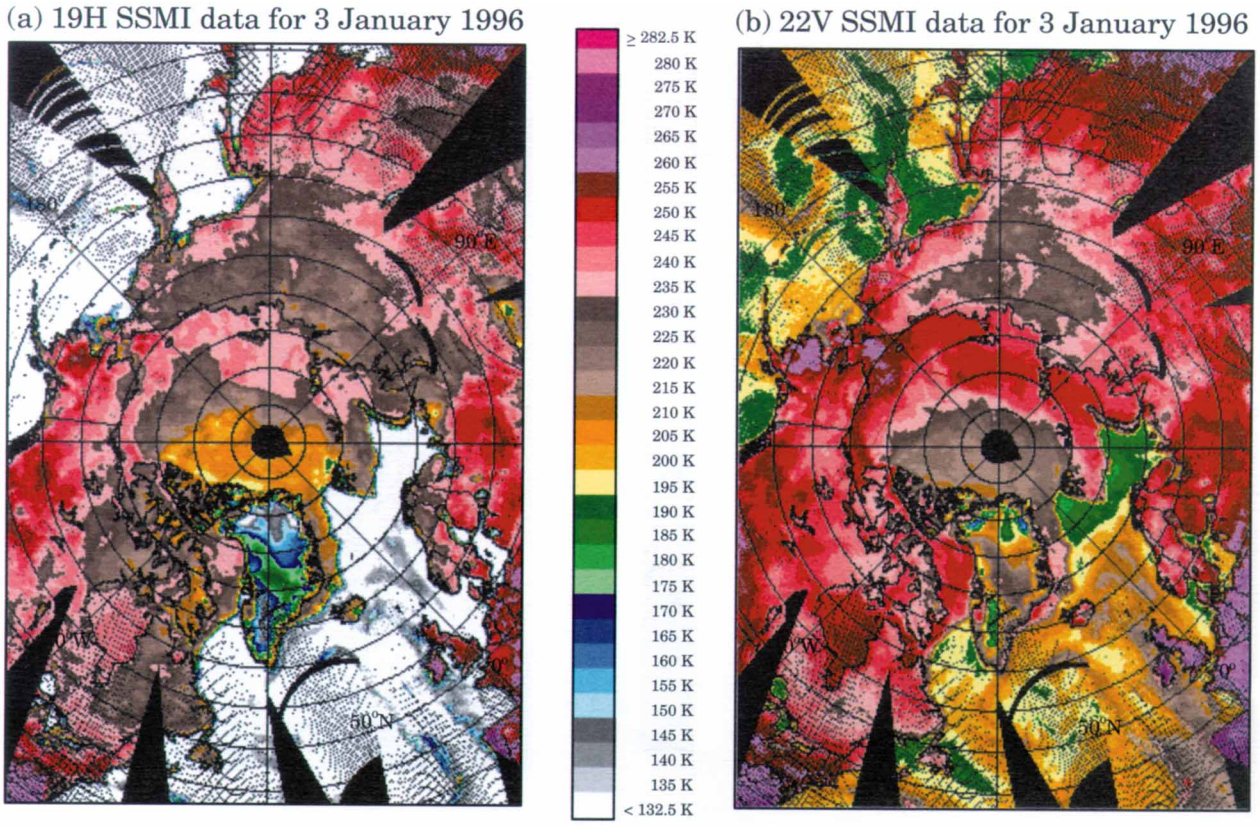

FIG. 1. Microwave brightness temperatures (K) for 3 January 1996, obtained from the DMSP SSMI for (a) 19.35 GHz horizontally polarized data, labeled 19H, and (b) 22.235 GHz vertically polarized data, labeled 22V. Locations with missing data are indicated in black.

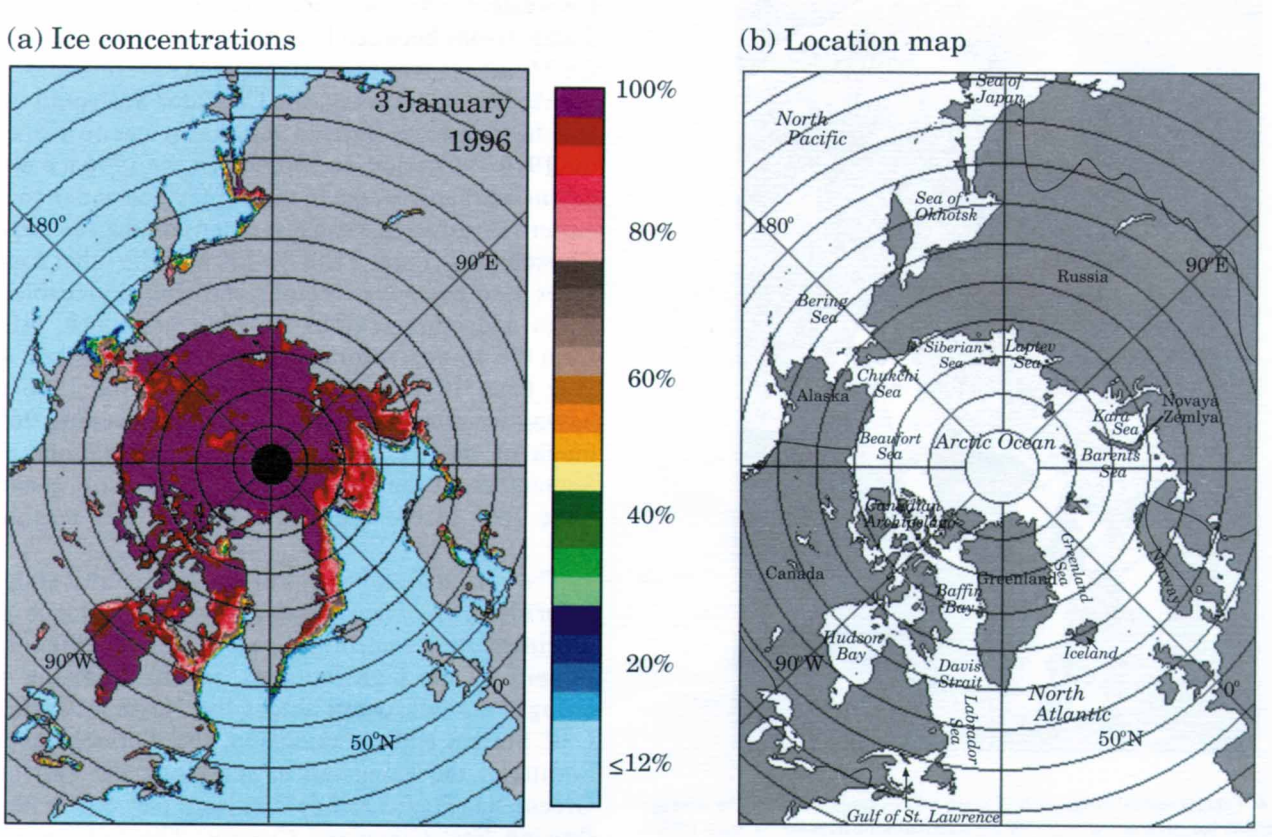

FIG. 2. (a) Sea ice concentrations for 3 January 1996, derived from the data of the DMSP SSMI. The black coloring filling the circular region poleward of 87.6°N indicates missing data caused by the satellite orbit. (b) Location map.

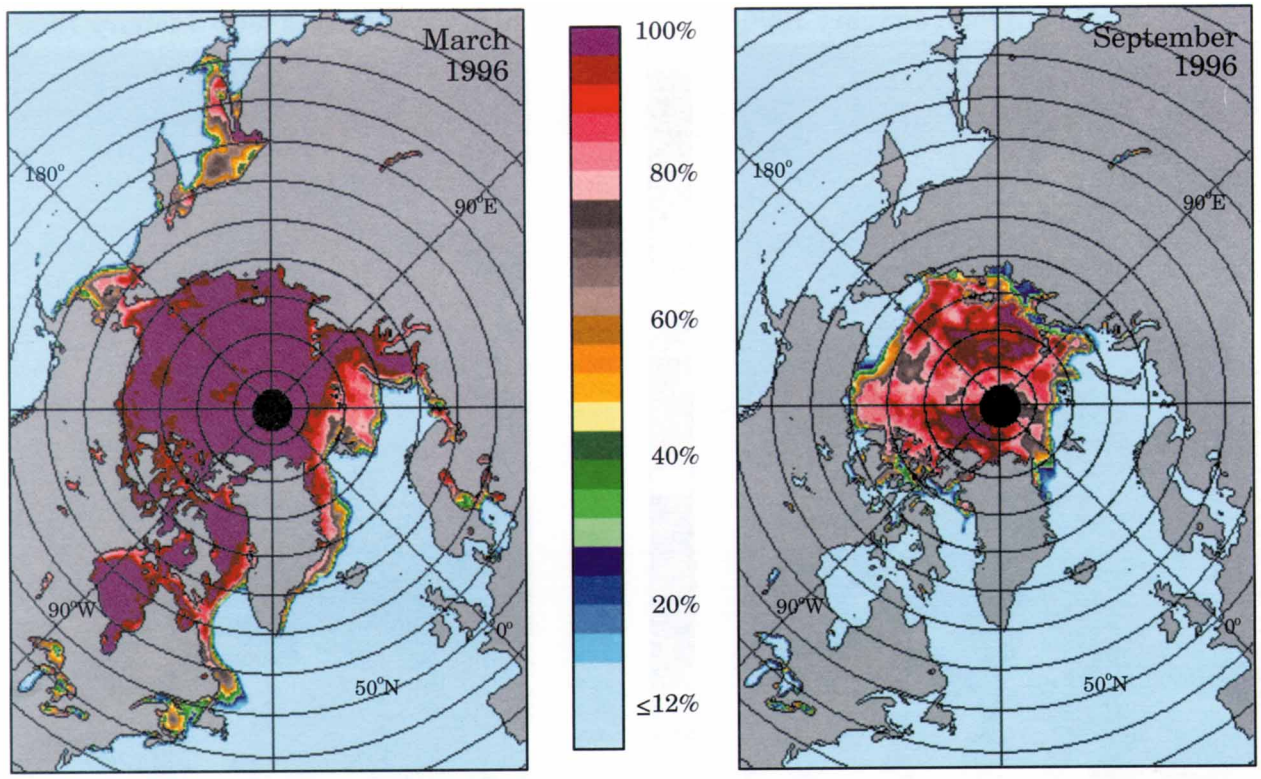

FIG. 3. Monthly average sea ice concentrations for March and September 1996, derived from the data of the DMSP SSMI. The black coloring filling the circular region poleward of 87.6°N indicates missing data caused by the satellite orbit.

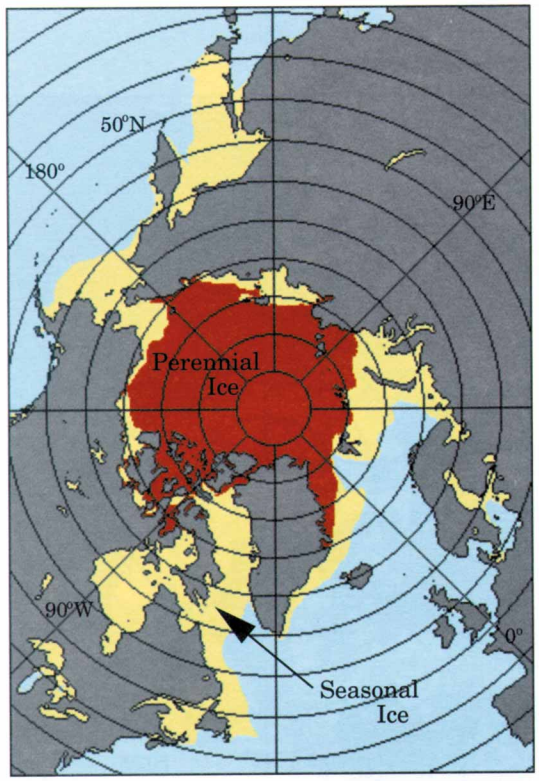

FIG. 4. Typical annual range of Arctic sea ice coverage, showing the average September ice coverage with ≥ 15% ice concentration over the 18 years 1979–96 (labeled "Perennial Ice") and the corresponding average March ice coverage (the combined "Perennial Ice" and "Seasonal Ice" regions). The ice coverages were derived from the data of the Nimbus 7 SMMR and the DMSP SSMIs.

the western Greenland Sea, and the northern Barents Sea. Comparisons between Figures 3 and 4 reveal that in 1996, the March ice was less extensive in several areas, including the Sea of Okhotsk, the Labrador Sea south of 50°N, and the far eastern Barents Sea, than it was on average over the 1979–96 period. In September, the 1996 ice was more extensive than average in the Laptev Sea and in the southeastern Beaufort Sea and less extensive than average in the Chukchi Sea (Figs. 3 and 4). Each of the other individual years also has some regions showing noticeable differences and other regions showing very little difference from the 18-year-average distributions of Figure 4. Each year from 1979 to 1996 is similar to the 1996 case in having ice concentrations in March exceeding 96% over much of the ice pack and ice concentrations even in September, at the ice extent minimum, still generally at least 76% in the reduced region of sea ice coverage (Fig. 3).

The spatial distributions of the ice are intricately tied to other elements of the climate system. For instance, the lack of wintertime ice north and west of Norway (Figs. 3 and 4), in spite of the high latitudes, results from the warmth brought northeastward across the North Atlantic by the Gulf Stream and its extension, the Norwegian Current. Similarly, the extension of ice along the east coast of Greenland (Figs. 3 and 4) is in large part due to the south-flowing East Greenland Current. The full ice coverage over Hudson Bay in winter (Figs. 3 and 4), in spite of its relatively low latitudes compared to most of the other

ice-covered regions, results from Hudson Bay's location in the midst of a continent. The continentality effect produces colder winters and warmer summers than those in open ocean expanses at the same latitudes.

Interannual Variability of Ice Coverage

Among the key aspects of the interannual variability of the ice cover is the variability in the overall distribution of the ice. Figures 5–7 present maps for each month that identify, in dark gray, those locations that have ice present in that month for some but not all of the 18 years 1979–96, i.e., the locations that are variable regarding the presence or absence of ice (on a monthly average basis) in the particular month. In all cases, ice is assumed to be present if the calculated ice concentration is at least 15% and absent if the calculated ice concentration is less than 15%. (The region from 84.6°N to 90°N, where the Nimbus 7 orbit prevented collection of SMMR data, is assumed to be ice covered to at least 15% ice concentration, and hence is colored white in Figures 5–7. This assumption is well justified, given that all the ice concentrations calculated adjacent to this region are consistently far higher than 15% on a monthly average basis.)

For each month, there is no variability (regarding the presence or absence of ice to a concentration of at least 15% in the 25 km × 25 km grid cells) throughout much of the central Arctic, where ice exists in each of the years, and there is no variability in most of the North Pacific and North Atlantic, where ice consistently does not exist (Figs. 5–7). Regarding simply the presence or absence of ice on a monthly average basis, the region of variability is located largely along the broad outer regions of the ice pack (Figs. 5–7). The main exception to this general statement occurs in June, when several scattered regions of variability exist (Fig. 6), reflecting the fact that as the ice begins to break up with the approach of summer, the breakup proceeds from within the pack in some regions. Probably the most studied of all such regions is the North Water Polynya area (e.g., Dunbar and Dunbar, 1972; Müller et al., 1977) to the west of Greenland at 76°–78°N. However increasing attention is now also being given (e.g., by Martin and Cavalieri, 1989; Brigham, 1996; Dethleff et al., 1998) to the polynya areas in the Russian Arctic seen in the June image of Figure 6 in the Laptev and East Siberian Seas. Because of the coarse spatial resolution of the images, only the larger polynyas are visible. Furthermore, the use of 18-year monthly averages masks the many temporary openings and closings of the polynyas and fails to show how early in the year they appear. For instance, the first month showing any hint of the North Water polynya in Figures 5–7 is May (Fig. 6), but in many years the polynya opens, at least temporarily, in each of the four previous months as well (e.g., Crawford and Parkinson, 1981).

For an example of the regional information contained in Figures 5–7, consider the Hudson Bay seasonal cycle. Hudson Bay is ice-covered throughout for the months January–April (Fig. 5) and remains largely ice-covered in May and June. Some minor variability occurs in May, with an occasional small offshore opening in the northwest. Much greater variability occurs in June, with open water in some years in the northwest, in some years in the east, and in some years in the far south (Fig. 6). In July, almost the entire bay exhibits variability: no location had ice in all 18 years, and only small regions in the southeast had consistently ice-free conditions (Fig. 6). In August, September, and October, most of the bay is consistently ice-free, whereas by December almost the entire bay is consistently ice-covered (Figs. 6 and 7). November is the ice-growth month with great variability (Fig. 7), similar to the level of variability in July. In the event of significant climate warming in the Hudson Bay region, variability would initially almost certainly increase in June and perhaps even in May, as ice breakup would presumably begin earlier. Similarly, variability would likely increase in December, as ice freeze-up would likely be delayed. Of course if the warming were to continue until ice no longer existed in June and December, then the subsequent ice-cover variability in those months (at least until the reemergence of ice) would be reduced to zero.

Frequency of Ice Coverage

To add detail to the regions of variability shown in Figures 5–7, maps have been generated showing the number of years of ice coverage for the months of ice maximum and minimum, March and September (Fig. 8). As in Figures 5–7, the area north of 84.6°N, without SMMR data, has been filled in as having ice to at least 15% ice concentration in all years. The white and light gray regions of the March and September images in Figures 5 and 7 are identical to the regions in Figure 8 mapped as having 18 and zero years of ice coverage, respectively, while the dark gray regions of Figures 5 and 7 are detailed in Figure 8 with 17 categories, ranging from a single year of ice coverage to 17 years of ice coverage.

Maps of the number of years of ice can be useful in identifying how unusual particular ice distributions or particular years are. For instance, of the years 1979–96, only one had monthly average September ice coverage extending to the northern tip of Novaya Zemlya (Fig. 8), so that particular September clearly had an unusually heavy ice coverage in that region. Inspection of the full set of 18 September maps (not shown) reveals that the extreme ice year in this region was 1980, shown in Figure 9. Similarly, only one of the years 1979–96 had ice-free September conditions north of 80°N at about 110°–130°E (Fig. 8), making it a year with unusually light ice conditions in that vicinity. The individual monthly maps show that year to be 1995 (Fig. 9). For a March example, only one year had ice in the Greenland Sea extending south to the north coast of Iceland (Fig. 8), and that year was 1979 (not shown here; visible in Gloersen et al., 1992, Fig. 3.1.18), the first year

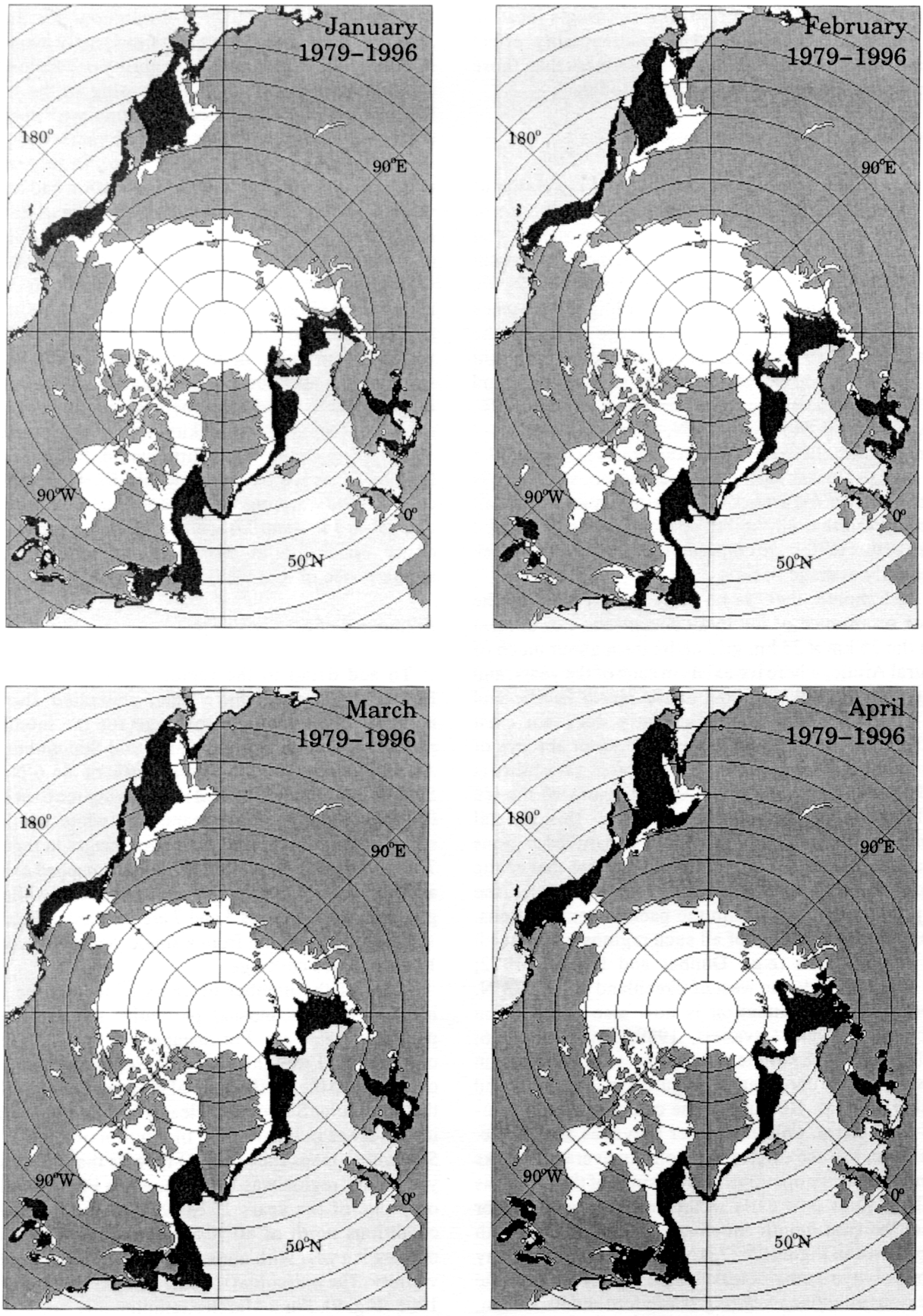

FIG. 5. Variability of monthly average sea ice distributions over the 18 years 1979–96, for the months January through April, as derived from the data of the Nimbus 7 SMMR and the DMSP SSMIs. White signifies the presence of ice of concentration ≥ 15% in each of the 18 years; dark gray signifies the presence of ice in some but not all years; and light gray signifies the consistent absence, on a monthly average basis, of ice of concentration ≥ 15%.

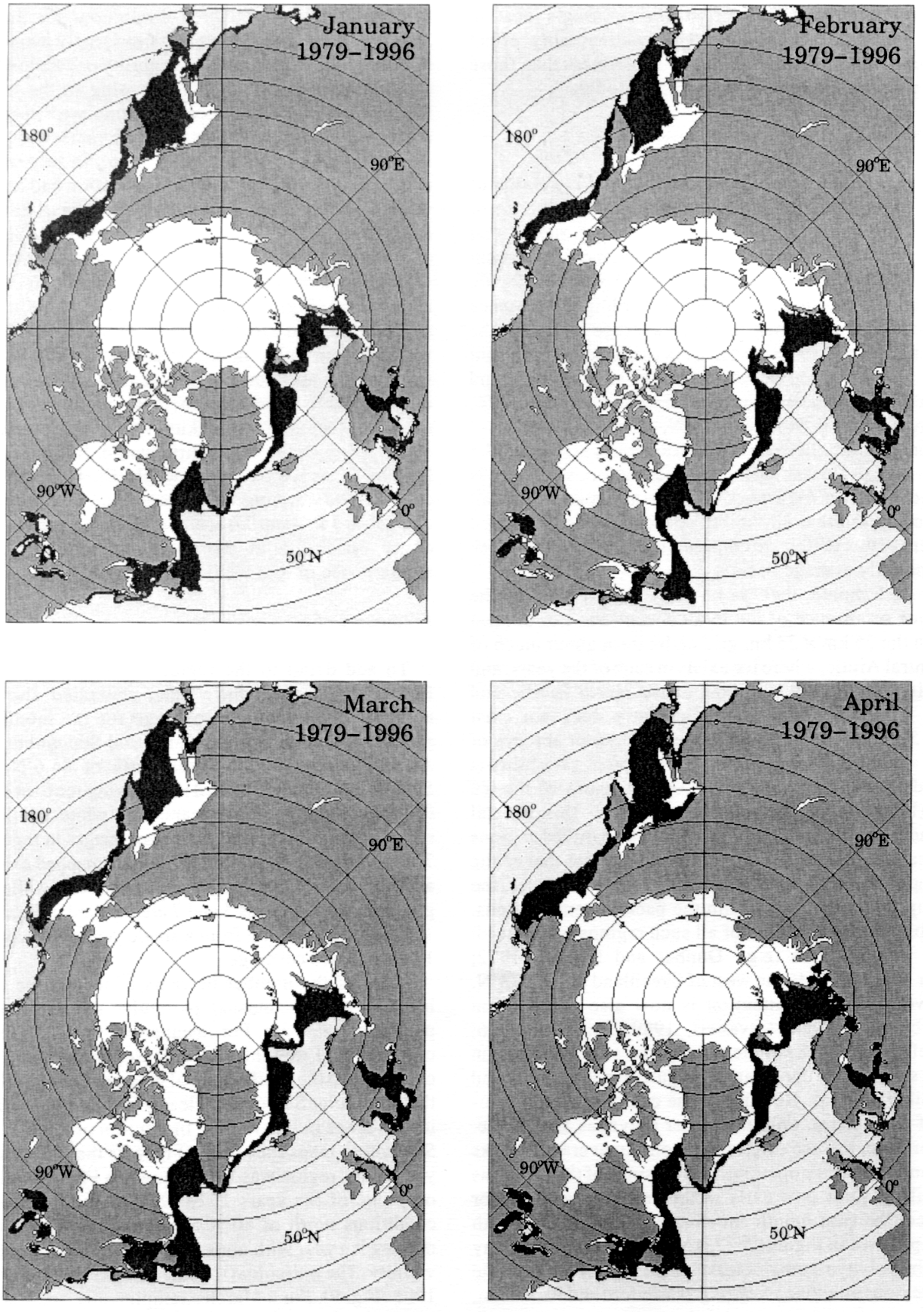

FIG. 6. Same as Figure 5 but for the months May through August.

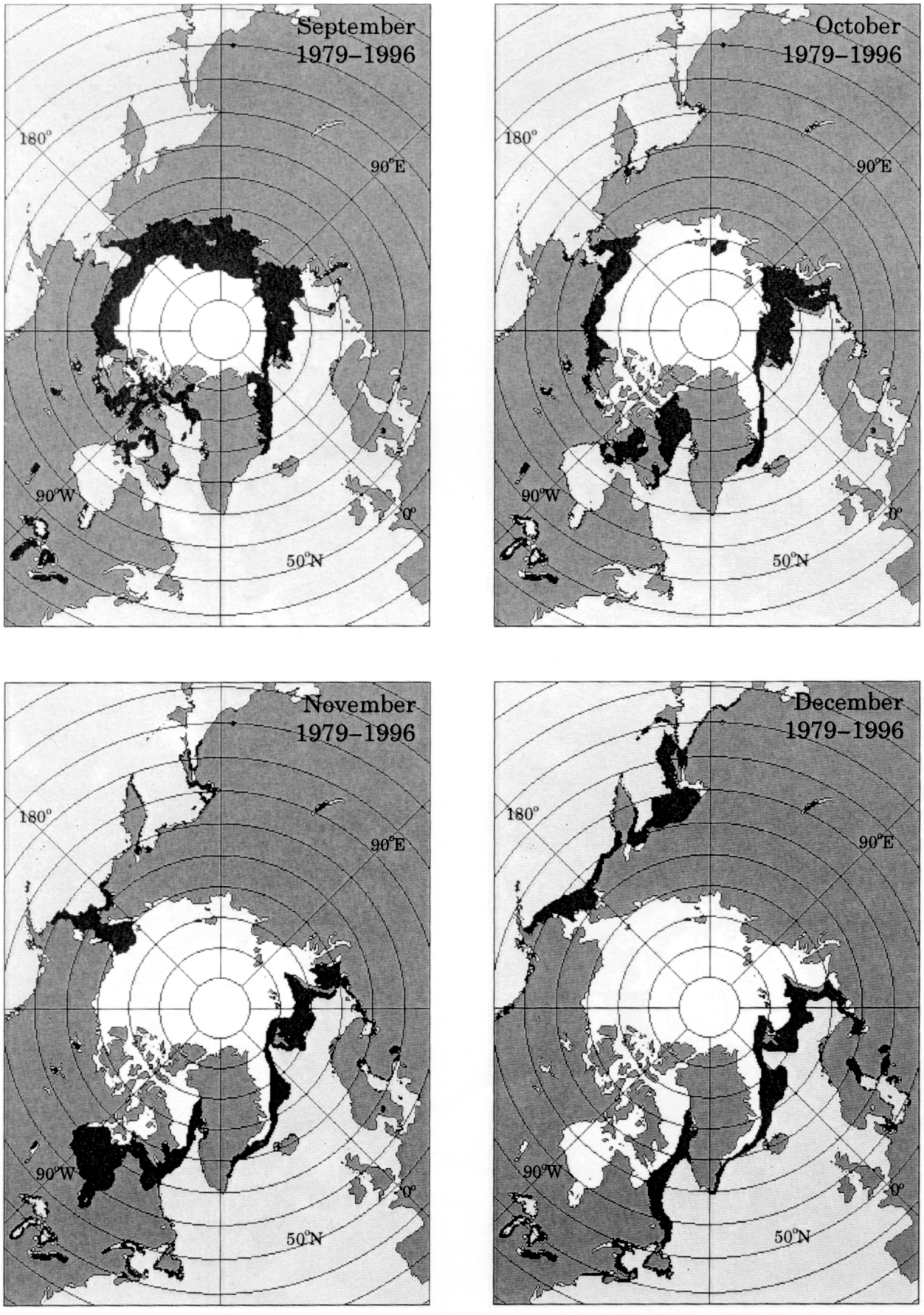

FIG. 7. Same as Figure 5 but for the months September through December.

of the data set and the same year that had particularly extensive ice in the southeastern Sea of Okhotsk and in the eastern Barents Sea (Fig. 8). However, although many of the unusually heavy ice conditions are in the early years and many of the unusually light ice conditions are in the later years of the data set, this is by no means consistently the case. For instance, the one year with practically no ice in March in the Gulf of St. Lawrence (Fig. 8) was 1981. Also, the unusually small ice coverage of September 1995 (Fig. 9 versus Fig. 4) was followed by much greater September ice coverage in 1996 (Fig. 3). In fact, for the 18-year record, September ice coverage was at its lowest in 1995, with an areal extent of 6.07×10^6 km^2, and at its second highest (second to 1980, Fig. 9) in 1996, with an extent of 7.55×10^6 km^2 (derived from the SMMR/SSMI record).

Maps of the number of years of ice were introduced in a paper by Parkinson (1991) that employed the ESMR and SMMR data through 1987 for March and through 1986 for September. The maps in Figure 8 follow the same format, incorporating the longer, 18-year SMMR/SSMI record. These maps, and the less detailed variability maps of Figures 5–7, can be highly relevant when considering reports of anomalous sea ice conditions, as they provide an easy means of placing new reports in the context of an 18-year record. They can, for instance, forestall unnecessary concerns over reports of excessive open water (with fears of a vanishing ice cover in the face of global warming) or excessive ice (with fears of a coming ice age) in cases when the distributions are found, upon comparison with Figures 5–8, to fall well within the variability observed in the past two decades. At the same time, these maps can also be important warning signals if indeed future ice conditions do fall noticeably outside the 1979–96 range. (Similar value can also derive from the much longer-term but far more localized data sets that exist for a few sea ice regions near inhabited areas, such as the record of the number of weeks per year with sea ice along the coast of Iceland, a record that is fairly complete back to 1600 and more spotty for the seven previous centuries [Koch, 1945]. The satellite record has the huge advantage of much greater spatial coverage, allowing assessment of patterns as well as the areal coverage of anomalous occurrences. The satellite record, however, is limited by its relative brevity.)

Length of the Sea Ice Season and 18-year Trends

Another measure of variability in the ice cover is the interannual variability in the number of days of ice coverage. This variable exerts a major impact on the heat, mass, and momentum exchanges between the ocean and the atmosphere, because the presence of an ice cover severely reduces such exchanges. Following Parkinson (1992), the variable is termed the "length of the sea ice season." It is not a "season" in the standard sense of constituting a continuous time interval but is instead defined, at each grid cell, as the number of days during the year when sea ice concentration was at least 15%. This definition reflects the total time of ice presence over the course of the year, automatically adjusting for periods with open-water polynyas (those days are not included in the "length of the sea ice season" total) and automatically avoiding the many issues associated with defining starting and ending dates for the sea ice season.

Figure 10 presents maps of the length of the sea ice season for 1979 and 1996, the starting and ending years of the data set. As in Figures 5–8, the missing-data region poleward of 84.6°N in the SMMR case and poleward of 87.6°N in the SSMI case has been filled in by the color of all the surrounding regions, in this case signifying an ice season lasting ≥ 359 days, which is well justified from all available in situ reports as well as from the satellite-derived results for the surroundings (Fig. 10). Clearly the Sea of Okhotsk and the eastern Barents Sea had much longer sea ice seasons in 1979 than in 1996, whereas Baffin Bay and portions of the Greenland Sea had longer sea ice seasons in 1996 than in 1979 (Fig. 10). In both years, sea ice coverage lasted throughout the year in most of the Arctic Ocean and well over half the year throughout most of Hudson Bay (Fig. 10).

Linear least squares trends through the 18 years of season-length data at each grid cell show the patterns of where, overall, the ice season lengthened and shortened (Fig. 11). These trends have been calculated both for season lengths defined as the number of days with at least 15% ice concentration, as in Figure 10, and for season lengths defined using a 30% cutoff instead. The welcome fact that the results are almost identical (Fig. 11) shows how little difference the precise choice of ice concentration cutoff makes. The Sea of Okhotsk, the central Greenland Sea, the eastern Barents Sea, and all the seas bordering the northern Russian coast all display shortening sea ice seasons; the strongest trends are in the eastern Barents Sea, and the largest coherent area of negative trends is in the Sea of Okhotsk (Fig. 11). The Chukchi Sea, the southern Canadian Arctic Archipelago, and northern Hudson Bay also show negative trends. Regions that experienced lengthening sea ice seasons instead are the Bering Sea, the eastern Beaufort Sea, northern and eastern Baffin Bay, Davis Strait, the Labrador Sea, the Gulf of St. Lawrence, and, to a lesser degree, central Hudson Bay (Fig. 11). (Results from the Canadian Arctic Archipelago are more suspect than those from the other regions because the Archipelago has so much less area far enough from land to be free of the contaminating influence of land radiation on the microwave radiation received by the satellite. The coarse resolutions, 25–50 km, of the passive-microwave data compound this problem, which would be less serious for higher resolution data.) Overall, considerably more of the ice-covered region experienced shortening sea ice seasons than lengthening ones: 7.5×10^6 km^2 had negative trends with magnitudes exceeding 0.5 days per year, and only 2.9×10^6 km^2 had positive trends exceeding 0.5 days per year (Fig. 11).

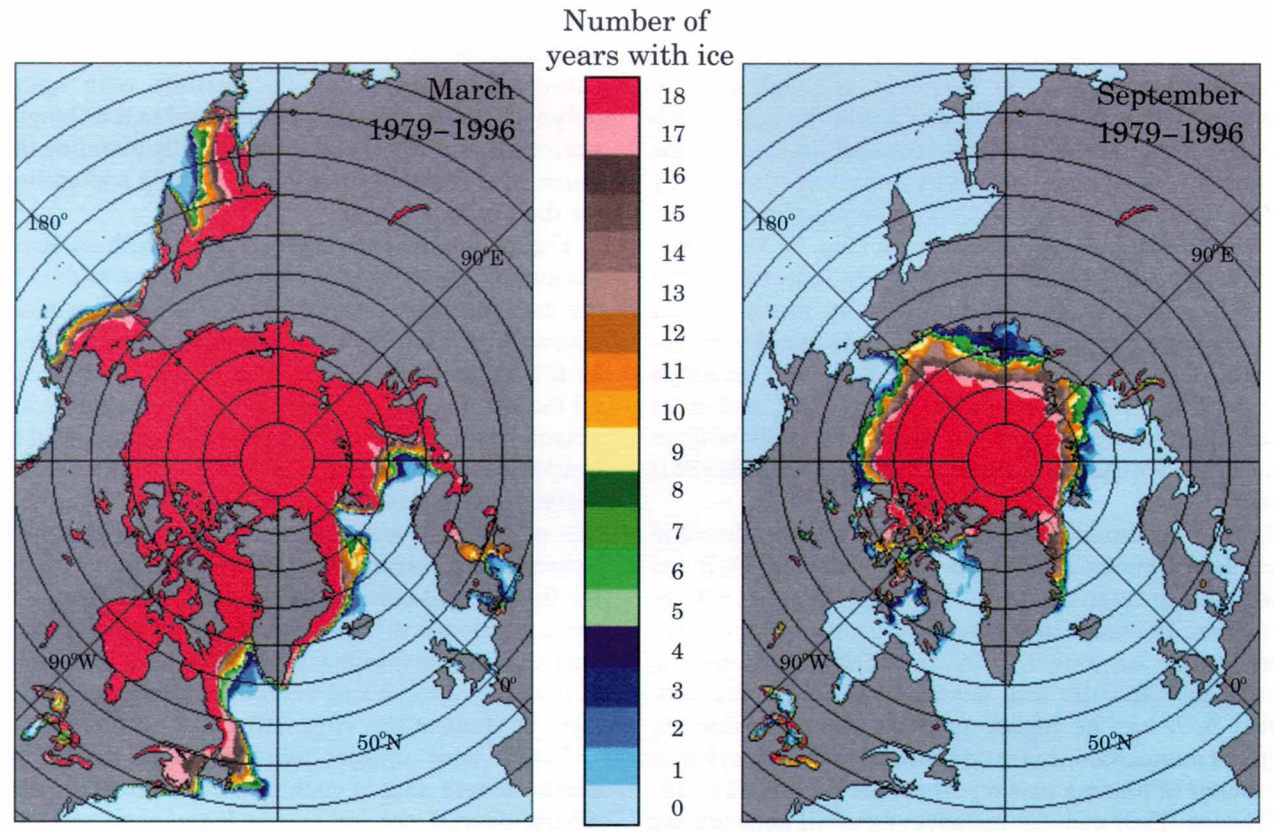

FIG. 8. Frequency of monthly average ice coverage (to a concentration of at least 15%) in March and September over the 18 years 1979–96, as derived from the data of the Nimbus 7 SMMR and the DMSP SSMIs.

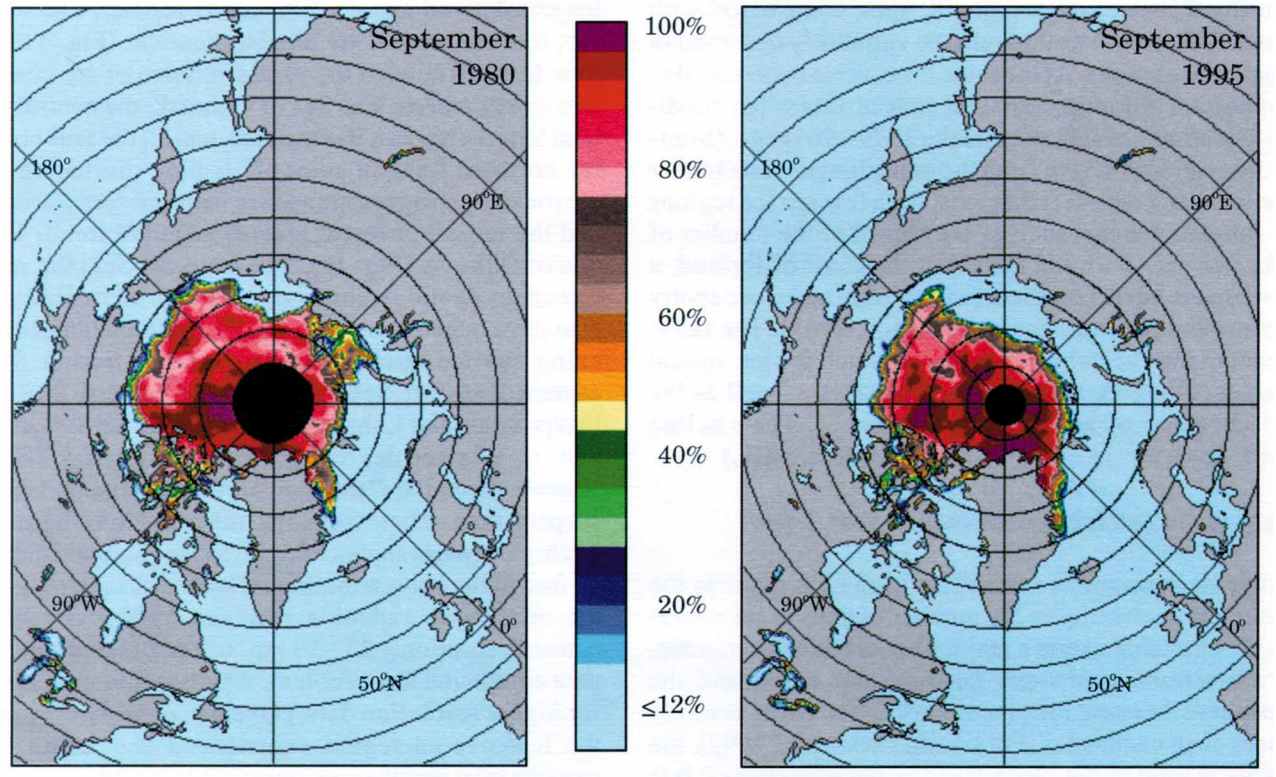

FIG. 9. Monthly average sea ice concentrations for September 1980, derived from the data of the Nimbus 7 SMMR, and for September 1995, derived from the data of the DMSP SSMI. The black coloring filling the circular regions poleward of 84.6°N in the 1980 image and poleward of 87.6°N in the 1995 image indicates missing data caused by the respective satellite orbits.

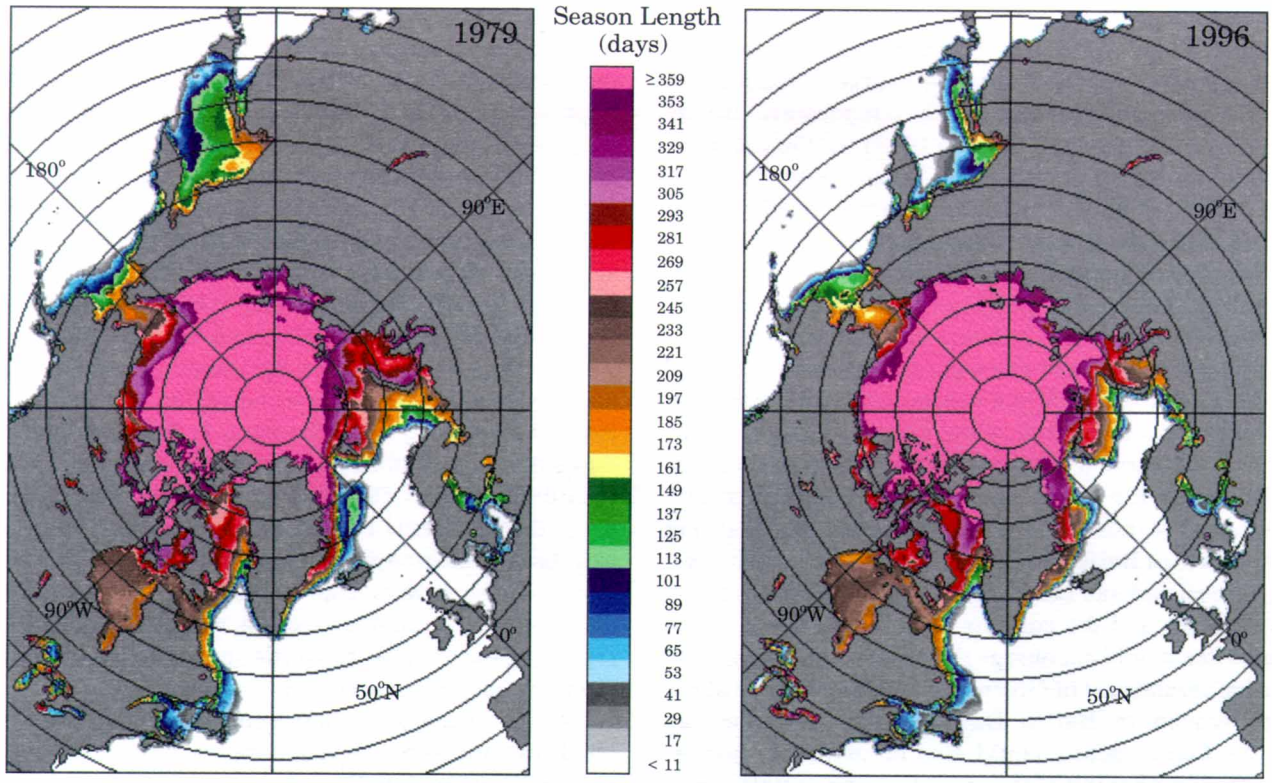

FIG. 10. Length of the sea ice season in 1979 and 1996, as determined by totaling (at each grid cell) the number of days with calculated sea ice concentration ≥ 15%, using the data of the Nimbus 7 SMMR for 1979 and the data of the DMSP SSMI for 1996.

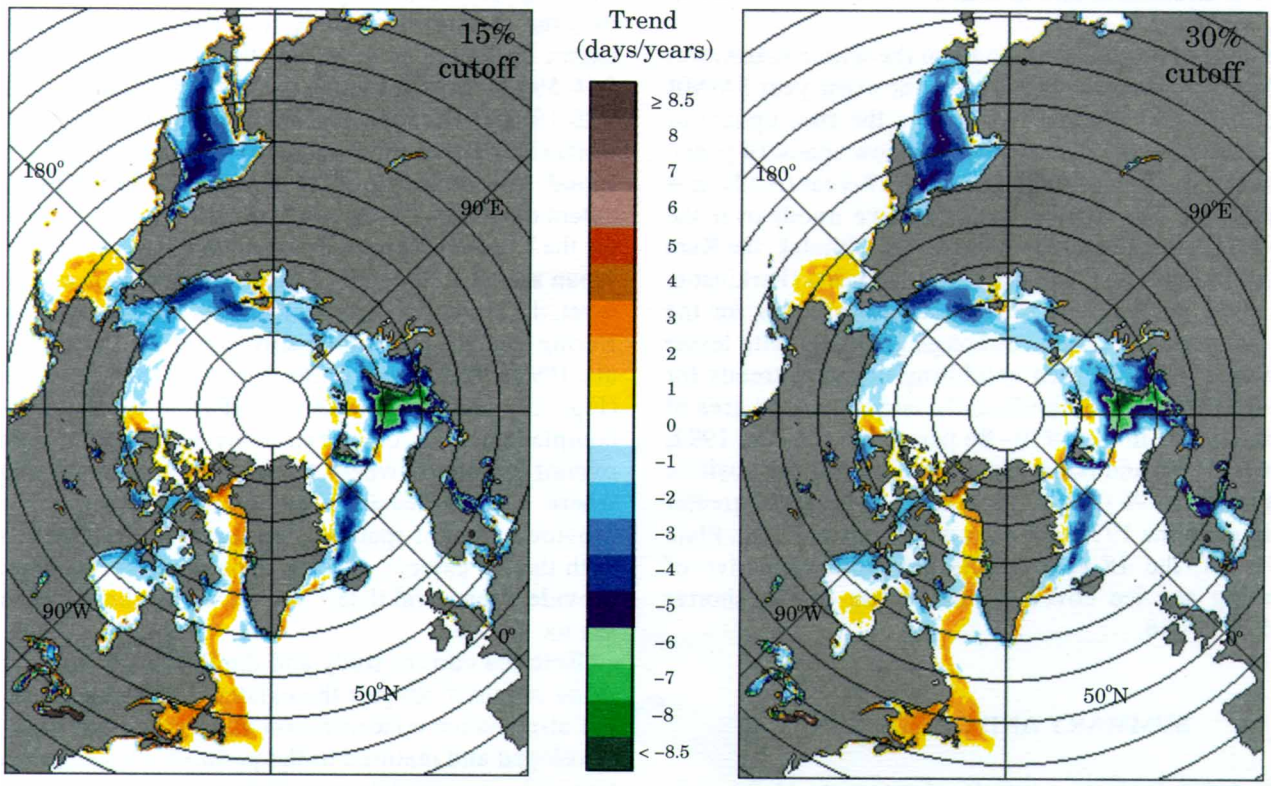

FIG. 11. Trends in the length of the sea ice season from 1979 through 1996, calculated at each grid cell as the slope of the line of linear least squares fit through the 18 years of season-length data. The trends are mapped for two ice concentration cutoffs: the left-hand image results from defining the length of the sea ice season as the number of days with calculated ice concentration ≥ 15%, as in Figure 10, and the right-hand image results from defining the length of the sea ice season as the number of days with calculated ice concentration ≥ 30%. All calculations are based on sea ice concentrations derived from the data of the Nimbus 7 SMMR and the DMSP SSMIs.

The fact of predominantly shortening sea ice seasons over much of the Arctic but lengthening sea ice seasons in the Baffin Bay, Davis Strait, and Labrador Sea regions (Fig. 11) corresponds well with temperature trends reported by Chapman and Walsh (1993) for the nonidentical but overlapping period 1961–90 and with the phase of the North Atlantic Oscillation during much of the SMMR/SSMI time period. Chapman and Walsh (1993) show warming over much of the Arctic but marked cooling over southern Greenland, Baffin Bay, Davis Strait, and the Labrador Sea. The North Atlantic Oscillation index, calculated as the normalized atmospheric pressure at Lisbon, Portugal, minus that at Stykkisholmur, Iceland, has been above average since 1980, with a strong Azores high-pressure system and a strong Icelandic low-pressure system (Hurrell, 1995). This combination results in strong southwesterly winds across the North Atlantic and strong north winds over Baffin Bay and the Labrador Sea (Hurrell, 1995; Hurrell and van Loon, 1997). The warm air over the North Atlantic and the cold air over Baffin Bay and the Labrador Sea would encourage the observed shortening of the sea ice season east of Greenland and lengthening of the sea ice season in Baffin Bay and the Labrador Sea (Fig. 11). Other factors could also be involved. For instance, the lengthening of the sea ice season in Baffin Bay and the Labrador Sea could instead result from a change in timing of the breakup of the ice bridge in Smith Sound (between Greenland and Ellesmere Island to its northwest).

Mapping of trends in the length of the sea ice season was first done in Parkinson (1992), for the eight-year SMMR period 1979–86. Figure 11 presents the first update of those results, with a data record that now spans 18 years. Comparing the 8-year trends with the 18-year trends, it is seen that: (1) The regions with negative trends over the 1979–86 period, centered on the Sea of Okhotsk, the Kara Sea, the Barents Sea, and the Greenland Sea (Parkinson, 1992, Plate 6), continue to have negative trends for the 1979–96 period (Fig. 11), although generally with lesser magnitudes. (2) The area exhibiting negative trends for 1979–96 (Fig. 11) is significantly larger than the area of negative trends in the 1979–86 period (Parkinson, 1992, Plate 6). (3) By and large, the regions exhibiting positive trends in 1979–96 (Fig. 11) had positive trends of greater magnitude in the 1979–86 period (Parkinson, 1992, Plate 6). Overall, the 18-year results are more reflective of decreasing sea ice coverage than those of the shorter period 1979–86.

SUMMARY AND DISCUSSION

This paper presents a variety of measures of the variability of Arctic sea ice distributions, all calculated from a recently completed 18-year data set of sea ice concentrations derived from the satellite passive-microwave observations of the Nimbus 7 SMMR and the DMSP F8, F11, and F13 SSMIs. Figures 4–8 and 11 give summary depictions of the variability of Arctic sea ice distributions for the period 1979–96, while Figures 2a, 3, 9, and 10 add illustrative details for individual months and years. The ice cover undergoes a large seasonal cycle (Figs. 3 and 4) and exhibits widespread interannual variability in each month (Figs. 5–8). Overall, a considerably larger area exhibits negative trends in the length of the sea ice season, suggestive of warming or increased ice advection away from the specific locality, than exhibits positive trends, suggestive of cooling or increased ice advection into the locality (Fig. 11). However, the trends are neither uniform nor monotonic, and rebounding of the ice cover can be marked from one year to the next, as demonstrated by the September ice conditions in the last two years of the data record: September 1995 had an unusually sparse ice coverage (Fig. 9 versus Fig. 4), but September 1996 (Fig. 3) had the second greatest September ice coverage of the 18 years. These results can be used in various ways, as discussed in the previous section, when considering issues regarding the state of the Arctic sea ice cover and possible climate changes involving it.

Sea ice extents and their trends have also been calculated from the same 18-year data set, and these have been analyzed both regionally and hemispherically in Parkinson et al. (1999). The ice extents correspond very well with the results in Figure 11 for the length of the sea ice season, showing an overall negative trend of -2.8% per decade over the 18 years for the Arctic as a whole. The largest ice extent decreases occurred in the Kara and Barents Seas (-10.5% per decade) and in the Seas of Okhotsk and Japan (-20.1% per decade). Ice extent increases found in the Baffin Bay/Labrador Sea and in the Bering Sea also correspond well with Figure 11. However, although the ice extent decreases for the north polar region as a whole and for the Kara and Barents Seas and the Seas of Okhotsk and Japan are all statistically significant at a 99% confidence level, the increases in the Baffin Bay/Labrador Sea and the Bering Sea are not statistically significant (Parkinson et al., 1999). The trends in the length of the sea ice season (Fig. 11) and the ice extents (Parkinson et al., 1999) complement each other extremely well, giving the same overall picture of where the ice cover is increasing and where it is decreasing, but the sea ice season results provide a level of spatial detail that is impossible to show with the ice extents, and the ice extents correspondingly provide a temporal detail not shown by the length of the sea ice season.

Both the current study and the Parkinson et al. (1999) study required not just the existence of the satellite data but also sea ice concentration algorithms that have been developed and matured to the point of allowing the creation of long-term data sets. Other variable aspects of the Arctic sea ice cover are also being examined from satellite data, although most of these remain at the research-development stage, so that long-term, validated data sets are not yet available for examining variability over a

TABLE 1. Selected references for other sea ice variables examined and mapped with satellite data.

Variable	Data sources[1]	References
Ice temperatures	SMMR and SSMI passive-microwave data	Gloersen et al. (1992) St. Germain and Cavalieri (1997)
	THIR infrared data	Comiso (1994)
	SSMI passive-microwave and AVHRR infrared data	Maslanik and Key (1993)
	AVHRR infrared and in situ data	Massom and Comiso (1994) Comiso and Kwok (1996)
Spring melt on the ice	DMSP visible and near-infrared data	Robinson et al. (1986)
	SMMR passive-microwave data	Anderson (1987)
	SAR active-microwave data	Winebrenner et al. (1994)
	DMSP visible, SMMR passive-microwave, and surface air temperature data	Serreze et al. (1993)
Ice types	SMMR passive-microwave data	Comiso (1986)
	AVHRR visible and infrared data	Massom and Comiso (1994)
	Landsat near-infrared data	Steffen and Heinrichs (1994)
	SAR active-microwave and Landsat visible and infrared data	Steffen and Heinrichs (1994)
	SAR active-microwave data	Fetterer et al. (1994)
	SAR active-microwave and SSMI passive-microwave data	Beaven and Gogineni (1998)
Melt-pond coverage	ESMR passive-microwave data	Carsey (1985)
Ice albedo	AVHRR visible and near-infrared data	Lindsay and Rothrock (1993)
	AVHRR visible data	Comiso and Kwok (1996)
Ice velocity fields	VHRR visible data	Muench and Ahlnas (1976)
	AVHRR visible data	Ninnis et al. (1986)
	AVHRR infrared data	Emery et al. (1991)
	SSMI passive-microwave data	Agnew et al. (1997); Kwok et al. (1998); Liu and Cavalieri (1998)
	NSCAT active-microwave data	Liu et al. (1998)
	SAR active-microwave data	Holt et al. (1992)

[1] Abbreviations: AVHRR = Advanced Very High Resolution Radiometer; DMSP = Defense Meteorological Satellite Program; ESMR = Electrically Scanning Microwave Radiometer; NASA = National Aeronautics and Space Administration; NSCAT = NASA Scatterometer; SAR = Synthetic Aperture Radar; SMMR = Scanning Multichannel Microwave Radiometer; SSMI = Special Sensor Microwave Imager; THIR = Temperature Humidity Infrared Radiometer; VHRR = Very High Resolution Radiometer.

decade or longer. Table 1 lists several of these variables, along with data sources used to examine them and references where readers can find details on methodology and sample results. The studies listed in Table 1 provide regional or larger-scale maps of these variables, demonstrating the potential of the satellite data and showing strong promise for eventual long-term data sets and routine monitoring from space. The reader is also referred to Carsey (1992) for additional uses of satellite microwave data for sea ice studies, to Tsatsoulis and Kwok (1998) for additional uses of satellite synthetic aperture radar (SAR) data, to Steffen et al. (1993) for snow and ice applications of Advanced Very High Resolution Radiometer (AVHRR) data, and to Massom (1991) for an overview and history of satellite sensing of the polar regions.

One extremely important Arctic sea ice variable that has not yet been measured from satellites is sea ice thickness. Ice thickness and ice concentration are the two key variables for determining sea ice volume—and hence sea ice mass—in the polar oceans. Determining changes in these two variables is critical for determining changes in the sea ice component of the climate system. But while ice concentrations have been calculated and mapped from satellite data since the 1970s (e.g., Figs. 2a, 3, and 9), the measurement of ice thicknesses from space remains a sought-after but elusive goal. Ice type derived from spaceborne SAR data has been used as a proxy indicator of ice thickness (Kwok et al., 1992); the formation of frost flowers determined from SAR data has been used to classify ice as having a thickness of 5–20 cm (Zabel et al., 1996); approximate ice thicknesses have been calculated for young ice using age determinations based on SAR data and a model of ice growth (Kwok, 1998); and inverse electromagnetic scattering models have been developed to determine sea ice thickness for thin sea ice, with the aim of eventual use with satellite data (Golden et al., 1998). However, no one has yet come close to direct measurement and monitoring of ice thickness from space. The importance of obtaining good thickness records has been highlighted by reports that sea ice thicknesses encountered by recent field expeditions, including the 1997–98 Surface Heat Budget of the Arctic (SHEBA) field program in the Beaufort Sea, have been unexpectedly low (e.g., McPhee et al., 1998) and by indications that submarine data suggest a possible thinning of portions of the Arctic ice (Wadhams, 1990). Development of a technique to measure sea ice thicknesses accurately from space would be a major contribution to the monitoring of the polar climate state and

hence to the determination of climate variability and climate change.

ACKNOWLEDGEMENTS

The 18-year record of sea ice concentrations used to derive the results presented in this paper was created through a team effort of the passive-microwave sea ice group at Goddard Space Flight Center (GSFC). Members of the science team are, in addition to the author of this paper, Don Cavalieri, Joey Comiso, Per Gloersen, and Jay Zwally. The GSFC team derived the ice concentrations from SMMR radiative data supplied by NASA and SSMI radiative data supplied by the National Snow and Ice Data Center (NSIDC) in Boulder, Colorado. We were also assisted at several stages by Jim Maslanik of NSIDC; and the compiled data set is now available through NSIDC. The figures for this paper were generated with the much-appreciated assistance of Jamila Saleh and John Eylander of Raytheon STX. Research funding was provided by NASA's Earth Observing System (EOS) Project Science Office and by NASA's polar program.

REFERENCES

AGNEW, T.A., LE, H., and HIROSE, T. 1997. Estimation of large-scale sea-ice motion from SSM/I 85.5 GHz imagery. Annals of Glaciology 25:305–311.

AINLEY, D.G., and DeMASTER, D.P. 1990. The upper trophic levels in polar marine ecosystems. In: Smith, W.O., Jr., ed. Polar oceanography, Part B: Chemistry, biology, and geology. San Diego: Academic Press. 599–630.

ANDERSON, M.R. 1987. The onset of spring melt in first-year ice regions of the Arctic as determined from scanning multichannel microwave radiometer data for 1979 and 1980. Journal of Geophysical Research 92(C12):13,153–13,163.

BEAVEN, S.G., and GOGINENI, S.P. 1998. Fusion of satellite SAR with passive microwave data for sea ice remote sensing. In: Tsatsoulis, C., and Kwok, R., eds. Analysis of SAR data of the polar oceans: Recent advances. Berlin: Springer. 91–109.

BRIGHAM, L.W. 1996. Sea ice and ocean processes in the Laptev Sea. Thesis for the degree of Master of Philosophy in Polar Studies. Scott Polar Research Institute, University of Cambridge, England. 93 p.

CARSEY, F.D. 1985. Summer Arctic sea ice character from satellite microwave data. Journal of Geophysical Research 90(C3): 5015–5034.

———., ed. 1992. Microwave remote sensing of sea ice. Geophysical Monograph 68. Washington, D.C.: American Geophysical Union. 462 p.

CAVALIERI, D.J., PARKINSON, C.L., GLOERSEN, P., COMISO, J.C., and ZWALLY, H.J. 1999. Deriving long-term time series of sea ice cover from satellite passive-microwave multisensor data sets. Journal of Geophysical Research 104(C7):15,803–15,814.

CHAPMAN, W.L., and WALSH, J.E. 1993. Recent variations of sea ice and air temperature in high latitudes. Bulletin of the American Meteorological Society 74(1):33–47.

COMISO, J.C. 1986. Characteristics of Arctic winter sea ice from satellite multispectral microwave observations. Journal of Geophysical Research 91(C1):975–994.

———. 1994. Surface temperatures in the polar regions from Nimbus 7 temperature humidity infrared radiometer. Journal of Geophysical Research 99(C3):5181–5200.

COMISO, J.C., and KWOK, R. 1996. Surface and radiative characteristics of the summer Arctic sea ice cover from multisensor satellite observations. Journal of Geophysical Research 101(C12):28,397–28,416.

CRAWFORD, J.P., and PARKINSON, C.L. 1981. Wintertime microwave observations of the North Water polynya. In: Gower, J.F.R., ed. Oceanography from Space. New York: Plenum Publishing. 839–844.

DETHLEFF, D., LOEWE, P., and KLEINE, E. 1998. The Laptev Sea flaw lead—detailed investigation on ice formation and export during 1991/1992 winter season. Cold Regions Science and Technology 27:225–243.

DUNBAR, M., and DUNBAR, M.J. 1972. The history of the North Water. Proceedings of the Royal Society of Edinburgh, Series B 72:231–241.

EMERY, W.J., FOWLER, C.W., HAWKINS, J., and PRELLER, R.H. 1991. Fram Strait satellite image-derived ice motions. Journal of Geophysical Research 96(C3):4751–4768, with corrections provided in 96(C5):8917–8920.

FETTERER, F.M., GINERIS, D., and KWOK, R. 1994. Sea ice type maps from Alaska Synthetic Aperture Radar Facility imagery: An assessment. Journal of Geophysical Research 99(C11):22,443–22,458.

GLOERSEN, P., CAMPBELL, W.J., CAVALIERI, D.J., COMISO, J.C., PARKINSON, C.L., and ZWALLY, H.J. 1992. Arctic and Antarctic sea ice, 1978–1987: Satellite passive-microwave observations and analysis. NASA SP-511. Washington, D.C.: National Aeronautics and Space Administration. 290 p.

GOLDEN, K.M., BORUP, D., CHENEY, M., CHERKAEVA, E., DAWSON, M.S., DING, K.-H., FUNG, A.K., ISAACSON, D., JOHNSON, S.A., JORDAN, A.K., KONG, J.A., KWOK, R., NGHIEM, S.V., ONSTOTT, R.G., SYLVESTER, J., WINEBRENNER, D.P., and ZABEL, I.H.H. 1998. Inverse electromagnetic scattering models for sea ice. IEEE Transactions on Geoscience and Remote Sensing 36(5):1675–1704.

GORNITZ, V., LEBEDEFF, S., and HANSEN, J. 1982. Global sea level trend in the past century. Science 215:1611–1614.

GRADINGER, R. 1995. Climate change and biological oceanography of the Arctic Ocean. Philosophical Transactions of the Royal Society of London, Series A 352:277–286.

GREBMEIER, J.M., SMITH, W.O., Jr., and CONOVER, R.J. 1995. Biological processes on Arctic continental shelves: Ice-ocean-biotic interactions. In: Smith, W.O., Jr., and Grebmeier, J.M., eds. Arctic oceanography: Marginal ice zones and continental shelves. Washington, D.C.: American Geophysical Union. 231–261.

HALPERT, M.S., and BELL, G.D. 1997. Climate assessment for 1996. Bulletin of the American Meteorological Society 78(5): S1–S49.

HANSEN, J., and LEBEDEFF, S. 1987. Global trends of measured surface air temperature. Journal of Geophysical Research 92(D11):13,345–13,372.

HOLT, B., ROTHROCK, D.A., and KWOK, R. 1992. Determination of sea ice motion from satellite images. In: Carsey, F.D., ed. Microwave remote sensing of sea ice. Geophysical Monograph 68. Washington, D.C.: American Geophysical Union. 343–354.

HORNER, R.A. 1989. Arctic sea-ice biota. In: Herman, Y., ed. The Arctic seas: Climatology, oceanography, geology, and biology. New York: Van Nostrand Reinhold. 123–146.

HURRELL, J.W. 1995. Decadal trends in the North Atlantic Oscillation: Regional temperatures and precipitation. Science 269:676–679.

HURRELL, J.W., and VAN LOON, H. 1997. Decadal variations in climate associated with the North Atlantic Oscillation. Climatic Change 36(3):301–326.

KARL, T.R., KNIGHT, R.W., and CHRISTY, J.R. 1994. Global and hemispheric temperature trends: Uncertainties related to inadequate spatial sampling. Journal of Climate 7:1144–1163.

KELLOGG, W.W. 1975. Climatic feedback mechanisms involving the polar regions. In: Weller, G., and Bowling, S.A., eds. Climate of the Arctic. Fairbanks, Alaska: Geophysical Institute, University of Alaska. 111–116.

KOCH, L. 1945. The East Greenland ice. Meddelelser om Grønland 130(3). 374 p.

KWOK, R. 1998. The RADARSAT geophysical processor system. In: Tsatsoulis, C., and Kwok, R., eds. Analysis of SAR data of the polar oceans: Recent advances. Berlin: Springer. 235–257.

KWOK, R., RIGNOT, E., HOLT, B., and ONSTOTT, R. 1992. Identification of sea ice types in spaceborne synthetic aperture radar data. Journal of Geophysical Research 97(C2): 2391–2402.

KWOK, R., SCHWEIGER, A., ROTHROCK, D.A., PANG, S., and KOTTMEIER, C. 1998. Sea ice motion from satellite passive microwave imagery assessed with ERS SAR and buoy motions. Journal of Geophysical Research 103(C4):8191–8214.

LINDSAY, R., and ROTHROCK, D. 1993. The calculation of surface temperature and albedo of Arctic sea ice from AVHRR. Annals of Glaciology 17:391–397.

LIU, A.K., and CAVALIERI, D.J. 1998. On sea ice drift from the wavelet analysis of the Defense Meteorological Satellite Program (DMSP) special sensor microwave imager (SSM/I) data. International Journal of Remote Sensing 19(7):1415–1423.

LIU, A.K., ZHAO, Y., and LIU, W.T. 1998. Sea-ice motion derived from satellite agrees with buoy observations. Eos, Transactions of the American Geophysical Union 79(30):353–359.

MARTIN, S., and CAVALIERI, D.J. 1989. Contributions of the Siberian shelf polynyas to the Arctic Ocean intermediate and deep water. Journal of Geophysical Research 94(C9): 12,725–12,738.

MASLANIK, J.A. 1992. Effects of weather on the retrieval of sea ice concentration and ice type from passive microwave data. International Journal of Remote Sensing 13(1):37–54.

MASLANIK, J., and KEY, J. 1993. Comparison and integration of ice-pack temperatures derived from AVHRR and passive microwave imagery. Annals of Glaciology 17:372–378.

MASSOM, R.A. 1988. The biological significance of open water within the sea ice covers of the polar regions. Endeavour, New Series 12(1):21–27.

———. 1991. Satellite remote sensing of polar regions: Applications, limitations and data availability. London: Belhaven Press. 307 p.

MASSOM, R., and COMISO, J.C. 1994. The classification of Arctic sea ice types and the determination of surface temperature using advanced very high resolution radiometer data. Journal of Geophysical Research 99(C3):5201–5218.

McPHEE, M.G., STANTON, T.P., MORISON, J.H., and MARTINSON, D.G. 1998. Freshening of the upper ocean in the Arctic: Is perennial sea ice disappearing? Geophysical Research Letters 25(10):1729–1732.

MELNIKOV, I.A. 1997. The Arctic sea ice ecosystem. Amsterdam: Gordon and Breach Science Publishers. 204 p.

MUENCH, R.D., and AHLNAS, K. 1976. Ice movement and distribution in the Bering Sea from March to June 1974. Journal of Geophysical Research 81(24):4467–4476.

MÜLLER, F., OHMURA, A., and BRAITHWAITE, R. 1977. The North Water Project (Canadian-Greenland Arctic). Polar Geography 1(1):75–85.

NINNIS, R.M., EMERY, W.J., and COLLINS, M.J. 1986. Automated extraction of pack ice motion from advanced very high resolution radiometer imagery. Journal of Geophysical Research 91(C9):10,725–10,734.

NSIDC (NATIONAL SNOW AND ICE DATA CENTER). 1992. DMSP SSM/I brightness temperatures and sea ice concentration grids for the polar regions on CD-ROM user's guide. NSIDC Special Report 1. Boulder, Colorado: NSIDC, Cooperative Institute for Research in Environmental Sciences, University of Colorado.

OELKE, C. 1997. Atmospheric signatures in sea-ice concentration estimates from passive microwaves: Modelled and observed. International Journal of Remote Sensing 18(5):1113–1136.

PARKINSON, C.L. 1991. Interannual variability of the spatial distribution of sea ice in the north polar region. Journal of Geophysical Research 96(C3):4791–4801.

———. 1992. Spatial patterns of increases and decreases in the length of the sea ice season in the north polar region, 1979–1986. Journal of Geophysical Research 97(C9):14,377–14,388.

PARKINSON, C.L., and KELLOGG, W.W. 1979. Arctic sea ice decay simulated for a CO_2-induced temperature rise. Climatic Change 2:149–162.

PARKINSON, C.L., COMISO, J.C., ZWALLY, H.J., CAVALIERI, D.J., GLOERSEN, P., and CAMPBELL, W.J. 1987. Arctic sea ice, 1973–1976: Satellite passive-microwave observations. NASA SP-489. Washington, D.C.: National Aeronautics and Space Administration. 296 p.

PARKINSON, C.L., CAVALIERI, D.J., GLOERSEN, P., ZWALLY, H.J., and COMISO, J.C. 1999. Arctic sea ice extents, areas, and trends, 1978–1996. Journal of Geophysical Research 104(C9):20,837–20,856.

RIND, D., HEALY, R., PARKINSON, C., and MARTINSON, D. 1995. The role of sea ice in 2 x CO_2 climate model sensitivity. Part I: The total influence of sea ice thickness and extent. Journal of Climate 8(3):449–463.

ROBINSON, D.A., SCHARFEN, G., SERREZE, M.C., KUKLA, G., and BARRY, R.G. 1986. Snow melt and surface albedo in the Arctic basin. Geophysical Research Letters 13(9):945–948.

SERREZE, M.C., MASLANIK, J.A., SCHARFEN, G.R., BARRY, R.G., and ROBINSON, D.A. 1993. Interannual variations in snow melt over Arctic sea ice and relationships to atmospheric forcings. Annals of Glaciology 17:327–331.

SMITH, S.L., and SCHNACK-SCHIEL, S.B. 1990. Polar zooplankton. In: Smith, W.O., Jr., ed. Polar oceanography, Part B: Chemistry, biology, and geology. San Diego: Academic Press. 527–598.

SMITH, W.O., Jr., and SAKSHAUG, E. 1990. Polar phytoplankton. In: Smith, W.O., Jr., ed. Polar oceanography, Part B: Chemistry, biology, and geology. San Diego: Academic Press. 477–525.

SPINDLER, M. 1990. A comparison of Arctic and Antarctic sea ice and the effects of different properties on sea ice biota. In: Bleil, U., and Thiede, J., eds. Geological history of the polar oceans: Arctic versus Antarctic. Amsterdam: Kluwer Academic Publishers. 173–186.

STEFFEN, K., and HEINRICHS, J. 1994. Feasibility of sea ice typing with synthetic aperture radar (SAR): Merging of Landsat thematic mapper and ERS 1 SAR satellite imagery. Journal of Geophysical Research 99(C11):22,413–22,424.

STEFFEN, K., BINDSCHADLER, R., CASASSA, G., COMISO, J., EPPLER, D., FETTERER, F., HAWKINS, J., KEY, J., ROTHROCK, D., THOMAS, R., WEAVER, R., and WELCH, R. 1993. Snow and ice applications of AVHRR in polar regions: Report of a workshop held in Boulder, Colorado, 20 May 1992. Annals of Glaciology 17:1–16.

ST. GERMAIN, K.M., and CAVALIERI, D.J. 1997. A microwave technique for mapping ice temperature in the Arctic seasonal sea ice zone. IEEE Transactions on Geoscience and Remote Sensing 35(4):946–953.

STIRLING, I. 1997. The importance of polynyas, ice edges, and leads to marine mammals and birds. Journal of Marine Systems 10:9–21.

STIRLING, I., and DEROCHER, A.E. 1993. Possible impacts of climate warming on polar bears. Arctic 46(3):240–245.

THOMPSON, L.G., MOSLEY-THOMPSON, E., DAVIS, M., LIN, P.N., YAO, T., DYURGEROV, M., and DAI, J. 1993. 'Recent warming': Ice core evidence from tropical ice cores with emphasis on Central Asia. Global and Planetary Change 7:145–156.

TSATSOULIS, C., and KWOK, R., eds. 1998. Analysis of SAR data of the polar oceans: Recent advances. Berlin: Springer. 290 p.

WADHAMS, P. 1990. Evidence for thinning of the Arctic ice cover north of Greenland. Nature 345:795–797.

WARRICK, R.A., LE PROVOST, C., MEIER, M.F., OERLEMANS, J., and WOODWORTH, P.L. 1996. Changes in sea level. In: Houghton, J.T., Meira Filho, L.G., Callander, B.A., Harris, N., Kattenberg, A., and Maskell, K., eds. Climate change 1995: The science of climate change. Contribution of Working Group 1 to the Second Assessment Report of the Intergovernmental Panel on Climate Change (IPCC). Cambridge, England: Cambridge University Press. 359–405.

WILLIAMS, R.S., Jr., and FERRIGNO, J.G., eds. 1989. Satellite image atlas of glaciers of the world: Glaciers of Irian Jaya, Indonesia, and New Zealand. U.S. Geological Survey Professional Paper 1386-H. Washington, D.C.: U.S. Geological Survey. 48 p.

———., eds. 1993. Satellite image atlas of glaciers of the world: Glaciers of Europe. U. S. Geological Survey Professional Paper 1386-E. Washington, D.C.: U.S. Geological Survey. 164 p.

WINEBRENNER, D.P., NELSON, E.D., COLONY, R., and WEST, R.D. 1994. Observation of melt onset on multiyear Arctic sea ice using the ERS 1 synthetic aperture radar. Journal of Geophysical Research 99(C11):22,425–22,441.

YOUNG, J.A.T., and HASTENRATH, S. 1991. Glaciers of Africa. In: Williams, R.S., Jr., and Ferrigno, J.G., eds. Satellite image atlas of glaciers of the world: Glaciers of the Middle East and Africa. U.S. Geological Survey Professional Paper 1386-G. Washington, D.C.: U.S. Geological Survey. G49–G70.

ZABEL, I.H.H., JEZEK, K.C., GOGINENI, S.P., and KANAGARATNAM, P. 1996. Search for proxy indicators of young sea ice thickness. Journal of Geophysical Research 101(C3):6697–6709.